ICTS #10.1080/03008207.2023.2275044, VOL 00, ISS 00

Acidosis induces significant changes to the murine supraspinatus enthesis organic matrix

Saparja Nag, Isabelle De Bruyker, Ashley Nelson, Mikayla Moody, Marla Fais and Alix C. Deymier

QUERY SHEET

This page lists questions we have about your paper. The numbers displayed at left are hyperlinked to the location of the query in your paper.

The title and author names are listed on this sheet as they will be published, both on your paper and on the Table of Contents. Please review and ensure the information is correct and advise us if any changes need to be made. In addition, please review your paper as a whole for typographical and essential corrections.

Your PDF proof has been enabled so that you can comment on the proof directly using Adobe Acrobat. For further information on marking corrections using Acrobat, please visit
http://journalauthors.tandf.co.uk/production/acrobat.asp;
https://authorservices.taylorandfrancis.com/how-to-correct-proofs-with-adobe/

The CrossRef database (www.crossref.org/) has been used to validate the references. Changes resulting from mismatches are tracked in red font.

AUTHOR QUERIES

Q1 The ORCID for "Isabelle De Bruyker" has been taken from CATS and verified against public API, and was found to be valid. Please Check.

Q2 Please provide the missing country for a affiliation .

Q3 Please provide the missing country for b affiliation .

Q4 Please provide the missing country for c affiliation .

Q5 Please provide missing Published online date.

Q6 Please note that the journal allows a maximum of "5" keywords. Please edit keywords accordingly.

Q7 No funding details have been found for your manuscript submission, so a Funding section has been added stating that no funding was received. Please correct if this is inaccurate.

Q8 The disclosure statement has been inserted. Please correct if this is inaccurate.

Q9 The CrossRef database (www.crossref.org/) has been used to validate the references. Please check and correct any mistakes.

Q10 Please provide missing Year of publication and author name or institution name for the [45] references list entry.

Q11 Please provide missing Year of publication, author name or institution name and Publisher name for the [49] references list entry.

Q12 Please provide missing page number for the [50] references list entry.

Q13 Please provide missing Year of publication for the [77] references list entry.

CONNECTIVE TISSUE RESEARCH
https://doi.org/10.1080/03008207.2023.2275044

Acidosis induces significant changes to the murine supraspinatus enthesis organic matrix

Saparja Nag[a], Isabelle De Bruyker[b], Ashley Nelson[b], Mikayla Moody[c], Marla Fais[b], and Alix C. Deymier[b,c]

[a]School of Medicine, University of Connecticut, Farmington, CT, USA; [b]Biomedical Engineering, University of Connecticut, Storrs, CT, USA; [c]Biomedical Engineering, University of Connecticut Health Center, Farmington, CT, USA

ABSTRACT

Rotator cuff pathology is a common musculoskeletal condition that disproportionately affects older adults, as well as patients with diabetes mellitus and chronic kidney disease. It is known that increased age and kidney dysfunction have been correlated to acidotic states, which may be related to the increased incidence of rotator cuff injury. In order to investigate the potential relationship between acidosis and rotator cuff composition and mechanics, this study utilizes a 14-day murine model of metabolic acidosis and examines the effects on the supraspinatus tendon-humeral head attachment complex. The elastic matrix in the enthesis exhibited significant changes beginning at day 3 of acidosis exposure. At day 3 and day 7 timepoints, there was a decrease in collagen content seen in both mineralized and unmineralized tissue as well as a decrease in mineral:matrix ratio. There is also evidence of both mineral dissolution and reprecipitation as buffering ions continually promote pH homeostasis. Mechanical properties of the tendon-to-bone attachment were studied; however, no significant changes were elicited in this 14-day model of acidosis. These findings suggest that acidosis can result in significant changes in enthesis composition over the course of 14 days; however, enthesis mechanics may be more structurally mediated rather than affected by compositional changes.

ARTICLE HISTORY
Received 3 May 2023
Accepted 13 October 2023

KEYWORDS
Acidosis; rotator cuff; biomechanics; elastosis; Raman spectroscopystructure-function

1 Introduction

Rotator cuff injuries affect over 20% of the population over 50 and over 50% of the population over 80[1]. These injuries cause pain, difficulty with work and everyday tasks, and disturbed sleep. This may lead to significant physical, emotional and financial burdens[2]. Rotator cuff tears are also difficult to repair, with post-surgical failure rates ranging from 20–90% depending on severity of the tear[3,4]. Despite this correlation between age and tear rate, it remains unclear what physiological factors may be responsible for this increased risk of rotator cuff tears. Significant evidence has shown that in addition to increased age, comorbidities like diabetes and chronic kidney disease (CKD) increase the risk of shoulder pain, frozen shoulder, spontaneous tendon ruptures, and inferior outcomes after rotator cuff arthroplasty[5–12]. Interestingly, all of these conditions are highly likely to exhibit acidosis as a comorbidity[13–15]. This suggests that acidosis may play a role in increasing the risk of tendon tears and ruptures.

Acidosis is defined as a condition in which the serum pH and bicarbonate (HCO_3^-) drops below normal physiological levels. It generally presents as a secondary condition to CKD and diabetes, affecting over 1.3 million people every year[16,17]. Acidosis has been shown to induce significant change in the composition and structure of bone, cartilage and tendon[18]. However, it is unknown how acidosis will affect the bone, fibrocartilage, and tendon present at the supraspinatus enthesis. Clinically, acidosis is associated with bone dissolution, leading to decreases in bone mineral density[19] and bone volume. There is additionally an increased rate of fracture[20] and functional limitations[21]. These bone defects are caused by bone dissolution and resorption[22–25]. With respect to tendon tissue, acidosis is associated with spontaneous tears and ruptures in clinical patients[26–28]. Studies have measured softening of tendons with acidosis[29] which may be related to acidosis-induced elastosis[26]. Despite this knowledge, it is unclear what mechanism causes changes to tendons with acidosis. Finally, a drop in pH has been associated with increased radiological joint destruction and the formation of granulocytes in hyaline cartilage in a clinical setting[26]. Although the effect on fibrocartilage has not been studied, decreased pH has been shown to cause a decrease in cartilage matrix synthesis, an increase in chondrocyte apoptosis,

CONTACT Alix C. Deymier deymier@uchc.edu Biomedical Engineering, University of Connecticut Health Center, 263 Farmington Ave, Biomedical Engineering, School of Dental Medicine, Farmington, CT 06030 USA

and reduced turnover of hypertrophic chondrocytes in the growth plate[30–32]. Although there is evidence that acidosis affects each of these tissues independently, how it affects the complex combination of these tissues found at the Supraspinatus-humeral head enthesis remains unknown.

In this study we use an established model of murine metabolic acidosis[23,33] to examine the compositional, structural, and mechanical changes induced by in vivo acid exposure in the supraspinatus-humeral head enthesis.

2 Methods

2.1 Induction of metabolic acidosis

All animal experimental procedures were approved by the Institutional Animal Care and Use Committee at UConn Health Center. 4–6-month-old male CD-1 mice (Charles River Laboratories, MA, n = 75) were randomly distributed 5 to a cage (as per UConn Health policy), racked by an independent veterinary assistant, and allowed to acclimate for 7 days. Then, five groups were each assigned three cages (n = 15): control, 1 day acidosis, 3 days acidosis, 7 days acidosis or 14 days acidosis based on their location on the racks. The four acidosis groups were administered ammonium chloride (NH_4Cl) and 5% sucrose in the drinking water starting at 0.2 M NH_4Cl on day 0 with a 0.1 M increase every 3 days up to 14 days as per our previously established model[22,23,33]. The mice in each acidosis subgroup (n = 15) were sacrificed on the appropriate day: day 1, 3, 7, and 14. Control mice (n = 15) were housed alongside the acidosis groups and were maintained on normal drinking water. The control mice were sacrificed throughout the study as previous data showed that 14 days of normal diet had no effect on the mice[23]. Blood pH and bicarbonate levels were measured via submandibular bleed immediately before sacrifice. These are reported in Figure 1. After sacrifice, the supraspinatus tendon-humeral head complexes were collected. Complexes from the right side of the animal were split into two groups and examined via (1) Raman Spectroscopy (n = 5 per group) and (2) Histology (n = 5 per group). Complexes from the left side were examined via (1) mechanics (n = 10–13 per group) followed by (2) microcomputed tomography (same samples as the mechanics). Group sizes were established based on results from previous work[34–37] assuming a power of 0.8 and a significance level of 0.05.

2.2 Raman spectroscopy

The mineral composition of the supraspinatus tendon-humeral head complex was determined using Raman spectroscopy (n = 5 per group) as has been previously done[35,36,38–40]. Supraspinatus tendon-humeral head complexes were dissected from thawed, freshly-frozen mice, embedded into Optimal Cutting Temperature (OCT), and frozen at −80 °C. Sagittal sections were cut via cryostat using the tape method[41], placed onto glass slides, and stored at −80 °C. Raman spectra were obtained using Witec α300 Raman spectrometer equipped with a 785 nm laser. Approximately 10–15 Raman measurements were obtained spaced at ~ 4–8 µm across the visualized tendon-to-bone attachment. Spectra were acquired with a 50X objective and an acquisition time of 45 × 2 sec. Each Raman spectra underwent cosmic-ray removal and background-correction using the Witec Program 5.1 software. The

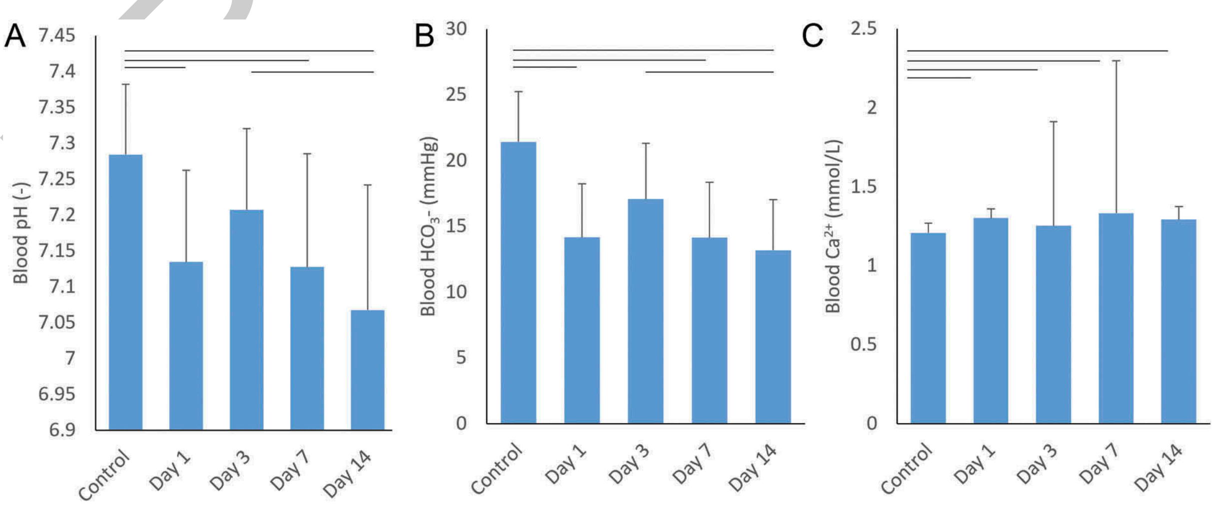

Figure 1. Blood gas results showing the changes in blood pH, HCO_3^-, and calcium content as a function of days of NH_4Cl administration. Bars represent p<0.05.

same software was used to fit the peaks of interest with Lorentzian curves to obtain the peak area, peak center location, and peak width of the peaks of interest. The peaks of interest were the 960 cm^{-1} ν_1 phosphate peak, the 1070 cm^{-1} carbonate peak, the 1450 cm^{-1} CH_2 bending peak, and the 1660 cm^{-1} amide I peak. The 1450 peak is associated with CH_2 vibrations in nearly all bone proteins and the 1660 peak is associated with amide I in the collagen environment; therefore, the 1660/1450 peak area ratio is used as a relative indicator of collagen content. The ratio of the 960/1450 peak areas was used to calculate the mineral:matrix ratio. Since phosphate is present in the apatite and CH_2 is present in nearly all bone matrix proteins, this provides information as to the relative bone mineral density. The 1070/960 peak area ratio is used to obtain the carbonate:phosphate ratio within mineralized tissue. Both the phosphate and carbonate that create these peaks are associated with the mineral; therefore, this ratio is representative of the relative amount of carbonate in the bone mineral. The peak center locations calculated from the fits of the peaks of interest were used to elucidate the molecular environment of those moieties. The full width of the peaks at half the maximum height (FWHM) were used as inverse indicators of the homogeneity of the molecular environment or the crystallinity of the mineral. These data are shown in Figures 2 and 3. Data acquisition was not blinded, but samples were randomized before collecting data to avoid variations in Raman acquisition between groups.

2.3 Histology

Following sacrifice, 5 supraspinatus tendon-humeral head complexes were dissected from each of the groups (control, day 1, day 3, day 7 and day 14). Samples were fixed in 4% paraformaldehyde (PFA), demineralized in 14% ethylenediaminetetraacetic acid (EDTA) for 12 days, and stored in 70% ethanol. Sections were then fixed in paraffin and sectioned. Blinded paraffin sections were stained using Trichrome to identify structural differences across the enthesis. The thickness of the mineralized fibrocartilage was measured from the subchondral bone to the mineralization tidemark. The thickness of the unmineralized fibrocartilage was measured from the tidemark to the beginning of the fibrous tendon. Six measurements were made for each tissue in each sample using ImageJ software. Structural

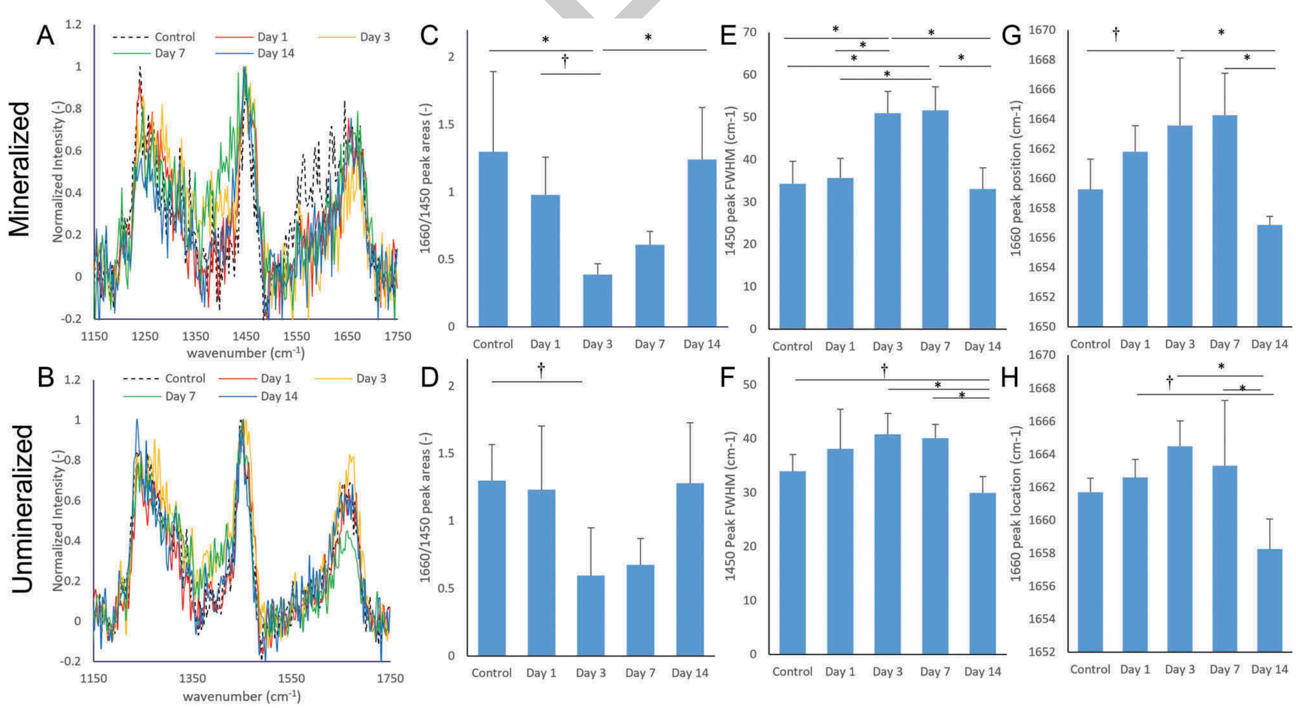

Figure 2. Raman outputs relative to the organic matrix of both mineralized and unmineralized tissues. The top row presents data associated with the mineralized tissues of the enthesis while the bottom row presents data for the unmineralized tissues. (A+B) representative Raman spectra of the 1240, 1450, and 1660 cm^{-1} peaks representing the amide III, CH_2 bending, and amide I moieties, respectively. (C+D) plots of the 1660/1450 ratio, which is representative of collagen content, as a function of time. (E+F) plots of the 1450 peak FWHM, which is inversely proportional to the atomic order of the organic matrix, as a function of time. (G+H) plots of the 1660 peak location, which is known to shift with collagen denaturation, as a function of time. * represents $p<0.05$ and † represents $p<0.1$.

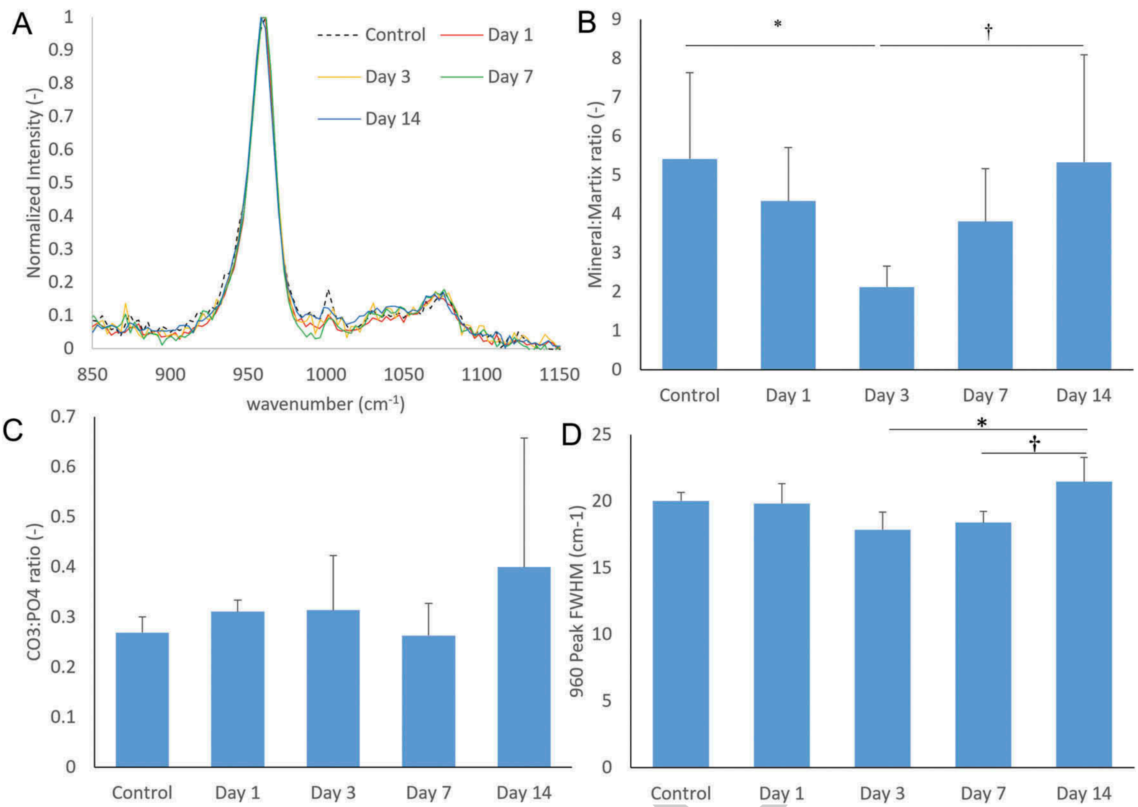

Figure 3. Raman outputs relative to the mineralized enthesis tissue. (A) representative Raman spectra of the 960 and 1070 cm^{-1} peaks associated with phosphate and carbonate in apatite, respectively. (B) plot of the mineral:Matrix ratio as a function of time. (C) plot of the carbonate to phosphate ratio (CO_3:PO_4) as a function of time. (D) plot of the 960 peak FWHM which is inversely proportional to the mineral crystallinity as a function of time. * represents p<0.05 and † represents p<0.1.

variations were determined visually by a blinded and trained observer. Sections were also stained with Verhoeff—Van Gieson (VVG) stain for elastic fibers and collagen[42–46]. For VVG staining, the area of the tendon was manually selected on randomized images by an experienced user. This area was then color thresholded in ImageJ to separate the pink collagen stain and the black elastic fiber stain. The black stained area was then calculated in ImageJ and normalized by the total selected tendon area to obtain the percentage Verhoeff -stained area of the tendon. This is an indicator of the amount of elastic fibers present in the sample. This data is shown in Figure 4.

2.4 Mechanics

Uniaxial tensile testing was conducted on thawed samples to determine the mechanical properties of the supraspinatus tendon-humeral head complex (n = 10–13 per group) according to established protocols[34,47–50]. Supraspinatus-humeral head complexes were dissected, and the supraspinatus muscle was removed from the supraspinatus tendon with blunt dissection. The humerus was placed into a custom 3D-printed cast to stabilize the diaphysis and the supraspinatus tendon was then placed into a custom aluminum clamp[50]. Testing was performed in a 37 °C phosphate-buffered saline bath installed on the Mach-1 mechanical tester with a 25 kg load cell.

Samples were loaded at a rate of 0.01 mm per second until failure. Locations of failure (enthesis, tendon bulk, or bony avulsion) were recorded for each sample. The force-displacement curve was used to calculate structural mechanical properties: maximum force, yield force, stiffness, and work. Gage length and tendon cross-sectional area, calculated from the micro-computed tomography, were utilized to produce stress-strain curves and calculate maximum stress, yield stress, modulus, resilience, and toughness. Values of stiffness and modulus were calculated by cyclic fitting of the linear-appearing region of the relevant curve with 10 points. The location of the 10 points was shifted with every cycle to maximize the R^2 value. The stiffness/modulus were calculated from the slope of the region with the greatest R^2 value ensuring that we are in the linear elastic region. Measures of yield were defined as the location at which the slope diverged from that determined for modulus/stiffness by more

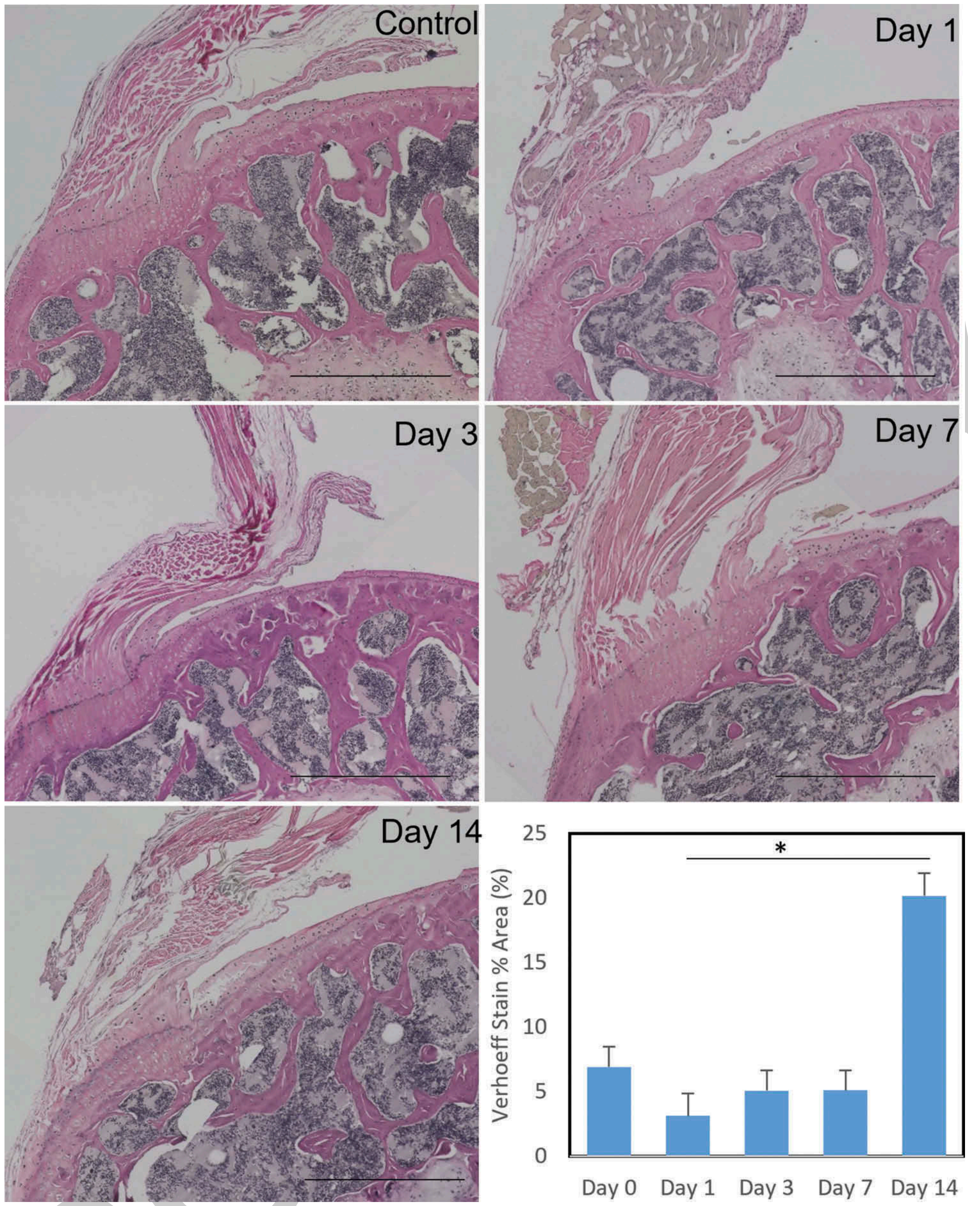

Figure 4. Representative images of the VVG staining for each time point accompanied by quantification of the unmineralized tissue percent area exhibiting Verhoeff staining. * represents p<0.05. Scale bars are 1 mm.

than 5%. Resilience and toughness were calculated from the area under the curve of the elastic and complete stress-strain curve, respectively. Data acquisition was not blinded, but samples were randomized before collecting data to avoid variations in mechanical testing parameters between groups.

2.5 Microcomputed-tomography

After mechanical testing, the bones and tendons were imaged via microcomputed tomography (μCT) (n = 10–13 per group). The tendons were stained with an iodine stain (10X dilution of 1% iodine metal (I2) and 2% potassium iodide (KI) in water) for approximately 18 hrs to increase contrast. All samples were scanned in a Scanco 50 μCT with a resolution of 16 μm. Bone characteristics were measured within the medial epiphysis of the humerus using CTAn (Bruker) to obtain bone volume, tissue volume, cortical thickness and trabecular parameters. The relative bone volume was calculated from the ratio of bone volume to total volume (BV/TV). Trabecular parameters include trabecular thickness (Tb.Th.), trabecular number (Tb.N.), and trabecular separation (Tb.Sp.) according to Dempster et al. and Parfitt et al[51,52]. This data is shown in Figure 5. Tendon cross-sectional area was measured along the entire length of the tendon to obtain mean and

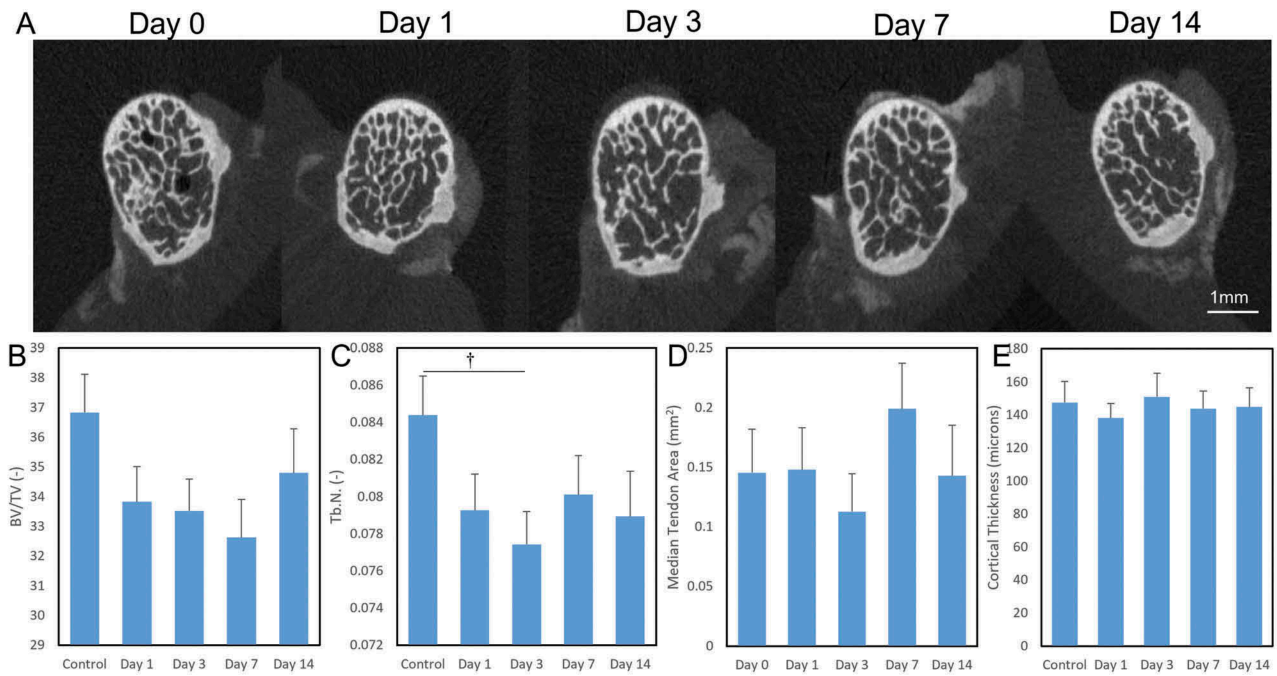

Figure 5. Structural effects of acidosis on the bone and tendon. (A) representative μCT images of the humeral epiphysis for each time point. (B) BV/TV as a function of time with acidosis. (C) plot of the trabecular number as a function of time. (D) plot of Median tendon area as a function of time. (E) plot of cortical thickness at the humeral epiphysis as a function of time. † represents $p<0.1$.

maximum cross-sectional values. Data acquisition was done blinded as was the analysis.

2.6 Statistics

All quantitative data was analyzed for normality and equal variance using the Shapiro-Wilk and Levene tests, respectively. Data which fulfilled both the requirements of normality and equal variance were analyzed using 1-way ANOVA with Tukey tests for means comparison. These datasets included the FWHM of the 960, 1450, and 1660 cm^{-1} peaks, the peak center location of the 1450 and 1660 cm^{-1} peaks, and all of the μCT data sets. Data that did not meet the requirements were analyzed using non-parametric Kruskal-Wallis testing with Dunn's tests for means comparison. These datasets include the mineral:matrix ratio, the carbonate:phosphate ratio, the 1660/1450 ratio, the 960 peak center location, all of the mechanical data, and the histological data. Testing was done using Origin Pro 2022. Significance was established at $p<0.05$ and trends are reported for $p<0.1$. Outliers were identified using Grubb's test and eliminated from datasets before statistical analysis if applicable. Plotted data is shown as mean ± standard deviation.

3 Results

3.1 Diet changes successfully induced and maintained acidosis in the mice

As previously reported for these mice[53], the graded addition of NH_4Cl successfully induced acidosis. The blood pH and HCO_3^- were both reduced compared to control at all days except day 3 (Figure 1A&B). The blood calcium was elevated at all days compared to controls (Figure 1C).

3.2 Acidosis affects the composition of both mineralized and unmineralized enthesis tissues

In terms of the organic matrix, we compared the effects of acidosis on both the composition of mineralized and unmineralized tissue (Figure 2A,B). The ratio of the 1660:1450 peak areas, which represent the collagen Amide I and protein CH_2 vibrations, were reduced at days 3 compared to control and day 14 in both mineralized and unmineralized tissues (Figure 2C,D). This suggests a reduction in collagen compared to the overall proteinaceous matrix. Similarly, the width of the 1450 peak generally increased in both the unmineralized and mineralized tissues at days 3 and 7 compared to control and day 14

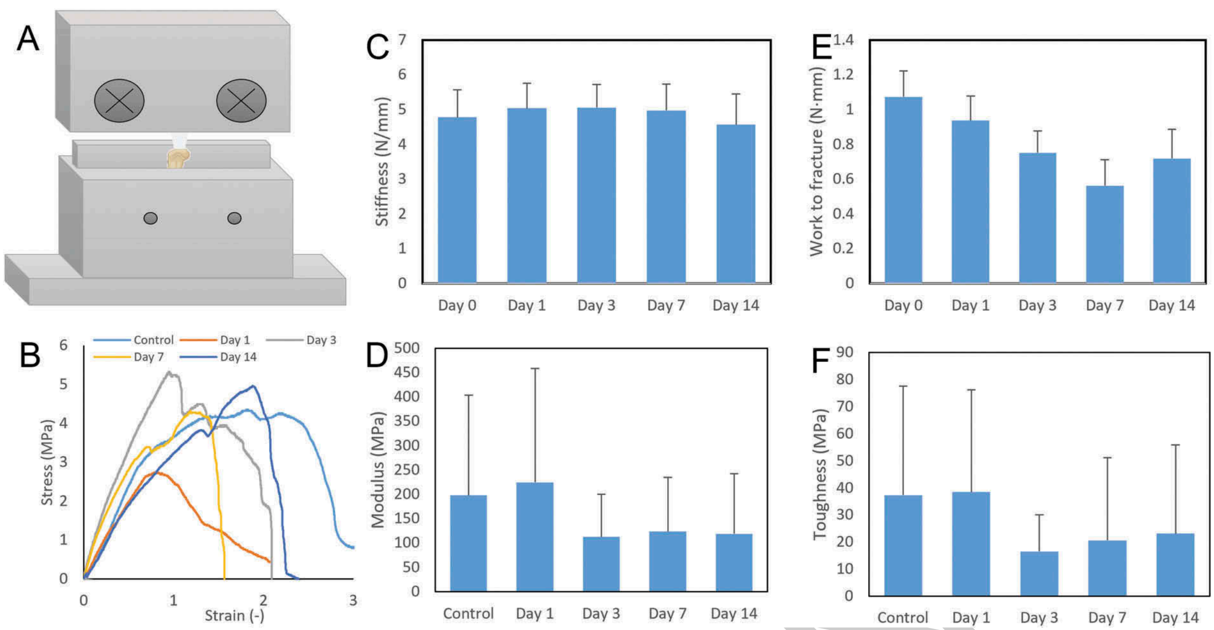

Figure 6. Mechanical responses to acidosis. (A) schematic showing the grip system used to mechanical load the supraspinatus tendon-humerus complex. (B) representative stress-strain diagrams for each timepoint. (C) plot of stiffness as a function of time. (D) plate of modulus as a function of time. (E) plot of work as a function of time (F) plot of toughness as a function of time. † represents $p<0.1$.

(Figure 2E,F). In the mineralized tissue, the peak center location of the 1450 peak was significantly reduced at days 3 and 7 compared to control groups (SFigure 1). The width of the 1660 peak was generally unaffected by the acid exposure (SFigure 1), although the peak center location was shifted to higher wavenumber at days 3 and 7 compared to day 14 (Figure 2G,H).

The mineral content, as determined from the ratio of mineral-to-matrix ratio, exhibited a decrease on day 3 compared to day 0 and 14 (Figure 3B). The mineral carbonate content showed no change with acidosis exposure (Figure 3C). However, the mineral crystallinity, as determined from the inverse of the 960 peak FWHM, was increased at days 3 and 7 compared to day 14 (Figure 3D). The location of the 960 peak center also had a trending increase at day 3 compared to day 14 (SFigure 1E).

3.3 Acidosis affects tendon elastin expression

Histologically, there were no significant morphological differences at the enthesis at varying days of acid exposure (SFigure 2). However, there were statistically significant differences between the expression of elastin as determined by Verhoeff's staining between day 1 and day 14 (Figure 4). At day 14, elastin expression increased nearly 3-fold compared to elastin expression in control samples.

3.4 Acidosis has minor effects on bone but not tendon architecture

Microcomputed tomography was used to determine the effects of acidosis on the architecture of the humeral head (Figure 5A). Acidosis only induced minor changes to the bone structure. Although there was no significant change in BV/TV (Figure 5B) there was a trending decrease in trabecular number at day 3 compared to controls (Figure 5C). Cortical thickness of the humeral epiphysis also remained unchanged (Figure 5E). Tendon cross-sectional area was not affected by acidosis exposure, as there was no significant difference in mean or maximum values (Figure 5D). The thickness of the mineralized and unmineralized fibrocartilage as well as the total fibrocartilage thickness at the supraspinatus-humerus enthesis was unchanged at any acidosis timepoint (SFigure 2).

3.5 Acidosis has no effects on the enthesis mechanics

Tensile testing of the supraspinatus-humerus complex indicated that there was no significant change in the structural or material mechanical properties of the enthesis. Neither the maximum force, maximum stress, stiffness, modulus, yield force, yield stress, work to fracture, nor toughness exhibited significant differences between time points (Figure 6 & SFigure 3).

4 Discussion

Clinically, acidosis is associated with reduced bone mineral density, increased fracture risk, and reduced functional outcomes[19,20,54]. As a result, the effects of acidosis on musculoskeletal tissues have been experimentally investigated for several decades[55–59]. However, most of these studies have focused on either long bones or calvarial tissue. This is despite the fact that clinical acidosis is also associated with increased tendon tears and ruptures[26,60,61]. Therefore, this study focused on the effects of a chronic acidosis state on the supraspinatus enthesis, with specific attention to the structure, composition, and mechanics of the enthesis site.

The mice in this study were maintained in acidosis via administration of NH_4Cl in the drinking water as per our established protocols[23]. As previously published, blood gas results show that the mice exhibited reduced blood pH and HCO_3^- at all timepoints except day 3 when the pH returned to control levels (Figure 1A, B)[22]. Blood calcium levels increased at all timepoints indicating that the acidosis is inducing bone dissolution (Figure 1C). To better understand the effects of acidosis and its compensatory mechanisms on the enthesis, its effects on the tissue composition, structure, and mechanics was investigated.

The biggest acidosis induced changes were compositional changes to the bone and tendon extracellular matrix. The 1660/1450 peak area ratio calculated from the Raman data, which is used here as a relative indicator of collagen content, was reduced at day 3 compared to control in both tendon and bone (Figure 2C,D). This suggests that the reduction in pH is causing a decrease in both tendon and bone collagen content. This could be due to a physiochemical response as collagen is known to be pH-dependent and undergo denaturation in acidic environments[62–64]. Collagen denaturation has been shown to reduce the area of the amide I subpeak for assembled collagen at 1640 cm^{-1} and increase the area for the amide I peak of denatured collagen at 1670 cm^{-1} leading to an overall shift in the total Amide I peak toward higher wavenumbers[65]. The Amide I peak location in the acidosis supraspinatus enthesis exhibits a shift toward 1670 cm^{-1} at day 3 compared to control (Figure 2G,H), suggesting that there may be an increase in collagen denaturation. Alternatively, there is evidence that acidosis inhibits collagen production by osteoblasts suggesting that there may also be cell-mediated processes affecting the tissue composition[66]. Additionally, the 1450 cm^{-1} peak width increased at days 3 and 7 compared to control, especially in the bone (Figure 2E,F). This peak is associated with bending of CH_2 bonds and therefore represents the broader organic extracellular matrix environment. An increase in the width of the 1450 cm^{-1} peak suggests that there is an increase in disorder or in the variety of organic moieties present in the tissue. As seen in Figure 2A, this broadening in the 1450 peak seems to be caused in part by increased signal between 1400–1440 cm^{-1}. Signal at this wavelength has been associated with hydrated denatured collagen[67]. However, increased signal in the 1420–1450 cm^{-1} region has also been associated with increased lipid content[68]. As acidosis has been shown to modify lipid metabolism and increase phospholipid formation, this broadening could be associated with increased lipid formation in the bone tissue[69]. Interestingly, the changes are significantly stronger in the bone tissue than in the tendon. This may be a result of increased fluid flow and vascularity in the bone tissue as compared to the tendon. Although there are significant changes in the organic matrix at day 3 and 7, the tissue appears to recover by day 14. It is unclear how the bone recovers despite the continued reduced blood pH. Due to the systemic induction of acidosis, it is possible that other mechanisms may be activated with time to minimize bone loss or protect against bone degradation.

Due to strong similarities in the elastin and collagen Raman spectra[67,70], Verhoeff's staining was used to identify the presence of elastic fibers in the tendon. Unlike the collagen which appears to undergo modifications at early time points, elastin levels increased significantly and rapidly at day 14 compared to day 1 (Figure 4). Chronic acidosis has been shown to increase elastic fiber staining in humans, known as elastosis, in the skin, lungs, cartilage, bone, and aorta as compared to control groups without chronic acidosis[71]. The origin of this increased elastin is not completely clear although there is some evidence that fibroblast extracellular matrix deposition may be affected by changes in pH[71]. Although the rapid change in ECM composition seems surprising, these types of rapid changes in elastic fiber content have been seen in other contexts such as in the aorta during the immediate perinatal period[72]. Here, there is a large increase in elastin content within 3 days of birth. Interestingly, this follows a spike in blood acidity measured at postnatal day 1[73]. In addition, similar increases in elastin have been reported clinically in the tendons of patients with acidosis or with conditions that co-present with acidosis such as chronic kidney disease[26,61]. These are associated with tendons ruptures or tears.

In addition to changes in the organic matrix of bone, there were also changes in the mineral content and crystallinity. The subchondral bone at the supraspinatus enthesis exhibits a decrease in mineral:matrix ratio at day 3 (Figure 3B), suggesting that there may be a loss of tissue mineral content at early acidosis timepoints. As previously mentioned, the mice exhibited reduced pH compared to controls at all timepoints except day 3 (Figure 1A). This trend toward mineral loss may point to an explanation for this return to pH homeostasis as bone dissolution is a known mechanism for the release of buffering ions to regulate pH[22–25]. Reduction in mineral content has also been measured in the femurs of mice exposed to the same acidosis regimen[22,23]. One of the buffering ions that is commonly released from bone is bicarbonate, HCO_3^-, which can result in a reduction of bone carbonate content. However, in this study there was no change in the relative CO_3:PO_4 ratio, suggesting that although there is mineral dissolution, there is not preferential removal of carbonate in the mineralized tissue (Figure 3C). However, the mineral does exhibit a decrease in the 960 cm^{-1} peak width, which is inversely proportional to the mineral crystallinity, at day 3 (Figure 3D). This points to dissolution of the mineral followed by reprecipitation into more crystalline crystals. This increase in crystallinity is associated with a decrease in mineral solubility, thus reducing its ability to continue supplying buffering ions to the system[74]. This reduction in solubility in addition to the increase in NH_4Cl dosage may explain the return to acidic blood pH in the following timepoints.

Structurally, when examining the effects of chronic acidosis on the supraspinatus tendon-humeral head enthesis via microcomputed tomography, minimal changes were seen in bone architecture. There was a trending decrease in trabecular number in the humeral epiphysis at day 3 of acidosis exposure when compared to control (Figure 5C). Similar decreases in femoral trabecular number at day 3 were also seen in mice exposed to the same acidosis regimen[22]. This is likely related to mineral loss measured using Raman spectroscopy and indicative of bone dissolution. Otherwise, there were no significant changes to either the trabecular or the cortical parameters (Figure 5C&E). Additionally, there were no significant changes to the tendon cross-sectional area (Figure 5D). In addition, there were no visible changes to the enthesis structure as determined from trichrome staining. This suggests that although there may be significant compositional changes to the enthesis tissue, there are no significant changes to the tissue structure.

Changes in collagen denaturation, elastin content, as well as mineral content and crystallinity have all been shown to affect tissue mechanics[26,74–77]. Therefore, it was necessary to examine the enthesis mechanics as a function of acidosis exposure. Despite all of the compositional changes, there were no significant changes to any of the mechanical properties of the enthesis at any time point (Figure 6). This suggests that the compositional changes measured here are either too small to affect whole tissue mechanics or that the enthesis mechanics is controlled by other factors. Studies looking at the effect of paralysis on enthesis mechanics suggested that it may be primarily controlled by bending of the cortical bone in the humeral head and its supporting trabecular architecture[35]. In this case, the lack of change in cortical thickness and BV/TV may maintain the tissue mechanics despite the compositional changes.

4.1 Limitations

The acidosis model used here maintains acidosis for 14 days. However, it is possible that continued acidosis could lead to enhanced elastosis and bone loss resulting in compromised bone mechanics. Therefore, it could be of interest to extend treatment to longer times in order to more fully replicate the effects of chronic acidosis in the mice.

5 Conclusions

In this study, acidosis was induced in mice using an established model of metabolic acidosis for 14 days. The acidosis had significant effects on the composition of the enthesis tissue especially in terms of the elastic matrix. At early time points (day 3 and 7), there were numerous changes suggesting that the acidosis causes dissolution and denaturation of collagen in both the bone and tendon compartments of the enthesis. This was followed by a rapid increase in elastin content in the tendon at Day 14. In addition to the changes in organic matrix, there was also a decrease in mineral content at days 3 and 7. This evidence of early mineral dissolution is in agreement with blood gas data. An increase in mineral crystallinity alongside the measured dissolution points to mineral dissolution/reprecipitation processes occurring in the mineralized enthesis. Despite these compositional changes, there are almost no significant changes to the enthesis structure or mechanics with acidosis. This suggests that the enthesis mechanics are more closely controlled by structural rather than compositional factors. Overall, these results point to significant and rapid compositional changes in the enthesis as a result of systemic acidosis. Although there were no mechanical modifications seen in this study, repeat cycles of acidosis—which are commonly seen with CKD, diabetes, and diet-induced acidosis—could lead to chronic modifications and long-term effects.

Acknowledgments

We would like to acknowledge the UConn Health Imaging and Histology Cores. SN was funded in part by the UConn Health Medical School Summer Research program. Funding was provided by AD's UConn Health Start-up fund and the NSF CAREER Grant (#2044870).

Disclosure statement

Q8 No potential conflict of interest was reported by the authors.

Funding

The author(s) reported there is no funding associated with Q7 the work featured in this article.

Data accessibility

All raw data is available upon request.

ORCID

Isabelle De Bruyker http://orcid.org/0009-0004-0540-495X

References

1. Tempelhof S, Rupp S, Seil R. Age-related prevalence of rotator cuff tears in asymptomatic shoulders. J Shoulder Elbow Surg. 1999;8(4):296–299. doi:10. Q9 1016/S1058-2746(99)90148-9.
2. Minns Lowe CJ, Moser J, Barker K. Living with a symptomatic rotator cuff tear 'bad days, bad nights': a qualitative study. BMC Musculoskelet Disord. 2014;15(1):Musculoskelet Disord 2014:15(228. doi:10.1186/1471-2474-15-228.
3. Harryman D, Mack L, Wang K, Jackins S, Richardson M, Matsen F. Repairs of the rotator cuff. Correlation of functional results with integrity of the cuff. J Bone Jt Surg. 1991;73(7):73(982–989. doi:10.2106/00004623-199173070-00004.
4. Galatz LM, Ball CM, Teefey SA, Middleton WD, Yamaguchi K. The outcome and repair integrity of completely arthroscopically repaired large and massive rotator cuff tears. J Bone Joint Surg Am. 2004;86(2):219–224. doi:10.2106/00004623-200402000-00002.
5. Akturk M, Karaahmetoglu S, Kacar M, Muftuoglu O. Thickness of the supraspinatus and biceps tendons in diabetic patients. Diab Care. 2002;25(2):408. doi:10.2337/diacare.25.2.408.
6. Bedi A, Fox AJ, Harris PE, Deng XH, Ying L, Warren RF, Rodeo SA. Diabetes mellitus impairs tendon-bone healing after rotator cuff repair. J Shoulder Elbow Surg. 2010;19(7):978–988. doi:10.1016/j.jse.2009.11.045.
7. Cho NS, Moon SC, Jeon JW, Rhee YG. The influence of diabetes mellitus on clinical and structural outcomes after arthroscopic rotator cuff repair. Am J Sports Med. 2015;43(4):991–997. doi:10.1177/0363546514565097.
8. Lin TT, Lin CH, Chang CL, Chi CH, Chang ST, Sheu WH. The effect of diabetes, hyperlipidemia, and statins on the development of rotator cuff disease: a nationwide, 11-year, longitudinal, population-based follow-up study. Am J Sports Med. 2015;43(9):2126–2132. doi:10.1177/0363546515588173.
9. Borton Z, Shivji F, Simeen S, Williams R, Tambe A, Espag M, Cresswell T, Clark D. Diabetic patients are almost twice as likely to experience complications from arthroscopic rotator cuff repair. Shoulder & Elbow. 2020;12(2):109–113. doi:10.1177/1758573219831691.
10. Arkkila PE, Kantola IM, Viikari JS, Rönnemaa T. Shoulder capsulitis in type i and ii diabetic patients: association with diabetic complications and related diseases. Ann Rheum Dis. 1996;55(12):907–914. doi:10.1136/ard.55.12.907.
11. Soyupek F, Demir M, Süslü FE, Baykal B, Sezer MT, Yesildag A. The upper extremity musculoskeletal complications in dialysis patients: comparison between hemodialysis and peritoneal dialysis. J Back Musculoskelet Rehabil. 2013;26(3):267–371. doi:10.3233/BMR-130375.
12. Shiota E, Tsuchiya K, Yamaoka K, Kawano O. Spontaneous major tendon ruptures in patients receiving long-term hemodialysis. Clin Orthop Relat Res. 2002;394:236–242. doi:10.1097/00003086-200201000-00028.
13. Frassetto L, Sebastian A. Age and systemic acid-base equilibrium: analysis of published data. J Gerontol: Series A. 1996;51A(1):B91–B99. doi:10.1093/gerona/51A.1.B91.
14. Raphael KL. Metabolic acidosis and subclinical metabolic acidosis in ckd. J Am Soc Nephrol. 2018;29(2):376–382. doi:10.1681/ASN.2017040422.
15. Kitabchi AE, Wall BM. Diabetic ketoacidosis. Med Clin North Am. 1995;79(1):9–37. doi:10.1016/S0025-7125(16)30082-7.
16. Benoit SR, Zhang Y, Geiss LS, Gregg EW, Albright A. Trends in diabetic ketoacidosis hospitalizations and in-hospital mortality - United States, 2000-2014. MMWR Morb Mortal Wkly Rep. 2018;67(12):362–365. doi:10.15585/mmwr.mm6712a3.
17. Kraut JA, Kurtz I. Metabolic acidosis of ckd: Diagnosis, clinical characteristics, and treatment. Am J Kidney Dis. 2005;45(6):978–993. doi:10.1053/j.ajkd.2005.03.003.
18. Levitt MF, Turner LB, Sweet AY, Pandiri D. The RESPONSE of BONE, CONNECTIVE TISSUE, and MUSCLE to ACUTE ACIDOSIS 12. J Clin Invest. 1956;35(1):98–105. doi:10.1172/JCI103256.
19. Tabatabai LS, Cummings SR, Tylavsky FA, Bauer DC, Cauley JA, Kritchevsky SB, Newman A, Simonsick EM, Harris TB, Sebastian A, Sellmeyer DE, et al. Arterialized venous bicarbonate is associated with lower bone mineral density and an increased rate of bone loss in older men and women. J Clin Endocr Metab. 2015;100(4):1343–1349. doi:10.1210/jc.2014-4166.
20. Sellmeyer DE, Stone KL, Sebastian A, Cummings SR. A high ratio of dietary animal to vegetable protein increases the rate of bone loss and the risk of fracture in postmenopausal women. Study of osteoporotic fractures research group. Am J Clin Nutr. 2001;73(1):118–122. doi:10.1093/ajcn/73.1.118.
21. Yenchek R, Ix JH, Rifkin DE, Shlipak MG, Sarnak MJ, Garcia M, Patel KV, Satterfield S, Harris TB,

Newman AB, Fried LF, et al. Association of serum bicarbonate with incident functional limitation in older adults. Clin J Am Soc Nephrol. 2014;9(12):2111–2116. doi:10.2215/CJN.05480614.
22. Moody M, Peterson A, Wingender B, Morozov K, Nakashima I, Easson M, Abraham R, Schmidt TA, Caromile L, Deymier AC. Physiochemical dissolution governs early modifications in acid-exposed murine bone with long-term recovery. Orthop Rheumatol. 2023;22(1):1–15. doi:10.19080/OROAJ.2023.22.556076.
23. Peterson AK, Moody M, Nakashima I, Abraham R, Schmidt TA, Rowe D, Deymier A. Effects of acidosis on the structure, composition, and function of adult murine femurs. Acta Biomater. 2021;121:121(484–496. doi:10.1016/j.actbio.2020.11.033.
24. Bushinsky DA, Krieger NS. Effects of acid on bone. Kidney Int. 2022;101(6):1160–1170. doi:10.1016/j.kint.2022.02.032.
25. Krieger NS, Frick KK, Bushinsky DA. Mechanism of acid-induced bone resorption. Curr Opin Nephrol Hypertens. 2004;13(4):423–436. doi:10.1097/01.mnh.0000133975.32559.6b.
26. Murphy KJ, McPhee I. Tears of major tendons in chronic acidosis with elastosis. J Bone Joint Surg Am. 1965;47(6):47(1253–1258. doi:10.2106/00004623-196547060-00018.
27. Bhole R, Flynn JC, Marbury TC. Quadriceps tendon ruptures in uremia. Clin Orthop Relat Res. 1985;195(&NA;):200–206. doi:10.1097/00003086-198505000-00023.
28. Jones N, Kjellstrand CM. Spontaneous tendon ruptures in patients on chronic dialysis. Am J Kidney Dis. 1996;28(6):861–866. doi:10.1016/S0272-6386(96)90386-8.
29. Kural Rahatli F, Turnaoglu H, Haberal KM, Kirnap M, Fidan C, Sayın CB, Uslu N, Haberal M. Acoustic radiation force impulse elastography findings of achilles tendons in patients on chronic hemodialysis and in renal transplant patients. Exp Clin Transplant. 2021;19(6):534–538. doi:10.6002/ect.2018.0015.
30. Wilkins RJ, Hall AC. Control of matrix synthesis in isolated bovine chondrocytes by extracellular and intracellular ph. J Cell Physiol. 1995;164(3):474–481. doi:10.1002/jcp.1041640305.
31. Zhou RP, Dai BB, Xie YY, Wu XS, Wang ZS, Li Y, Wang ZQ, Zu SQ, Ge JF, Chen FH. Interleukin-1β and tumor necrosis factor-α augment acidosis-induced rat articular chondrocyte apoptosis via nuclear factor-kappab-dependent upregulation of asic1a channel. Biochim Biophys Acta Mol Basis Dis. 2018;1864(1):162–177. doi:10.1016/j.bbadis.2017.10.004.
32. Carbajo E, López JM, Santos F, Ordóñez FA, Niño P, Rodríguez J. Histologic and dynamic changes induced by chronic metabolic acidosis in the rat growth plate. J Am Soc Nephrol. 2001;12(6):1228–1234. doi:10.1681/ASN.V1261228.
33. Liu Y, Atiq A, Peterson A, Moody M, Novin A, Deymier AC, Afzal J, Kshitiz. Metabolic acidosis results in sexually dimorphic response in the heart tissue. Metabolites. 2023;13(4):549. doi:10.3390/metabo13040549.
34. Deymier AC, Schwartz AG, Lim C, Wingender B, Kotiya A, Shen H, Silva MJ, Thomopoulos S. Multiscale effects of spaceflight on murine tendon and bone. Bone. 2020;131(115152):115152. doi:10.1016/j.bone.2019.115152.
35. Deymier AC, Schwartz AG, Cai Z, Daulton TL, Pasteris JD, Genin GM, Thomopoulos S. The multiscale structural and mechanical effects of mouse supraspinatus muscle unloading on the mature enthesis. Acta Biomater. 2019;83:83(302–313. doi:10.1016/j.actbio.2018.10.024.
36. Deymier-Black AC, Pasteris JD, Genin GM, Thomopoulos S. Allometry of the tendon enthesis: mechanisms of load transfer between tendon and bone. J Biomech Eng. 2015;137(11):111005–111005. doi:10.1115/1.4031571.
37. Peterson AK, Moody M, Nakashima I, Abraham R, Schmidt TA, Rowe D, Deymier A. Effects of acidosis on the structure, composition, and function of adult murine femurs. Acta Biomater. 2020;121:484–496. doi:10.1016/j.actbio.2020.11.033.
38. Schwartz AG, Lipner JH, Pasteris JD, Genin GM, Thomopoulos S. Muscle loading is necessary for the formation of a functional tendon enthesis. Bone. 2013;55(1):44–51. doi:10.1016/j.bone.2013.03.010.
39. Schwartz AG, Pasteris JD, Genin GM, Daulton TL, Thomopoulos S, Roeder RK. Mineral distributions at the developing tendon enthesis. PloS One. 2012;7(11):9. doi:10.1371/journal.pone.0048630.
40. Wopenka B, Kent A, Pasteris JD, Yoon Y, Thomopoulos S. The tendon-to-bone transition of the rotator cuff: a preliminary raman spectroscopic study documenting the gradual mineralization across the insertion in rat tissue samples. Appl Spectrosc. 2008;62(12):1285–1294. doi:10.1366/000370208786822179.
41. Dyment NA, Jiang X, Chen L, Hong S-H, Adams DJ, Ackert-Bicknell C, Shin D-G, Rowe DW. High-throughput, multi-image cryohistology of mineralized tissues. JoVe (J Visualized Exp). 2016; 115:e54468.
42. Caldini EG, Caldini N, De-Pasquale V, Strocchi R, Guizzardi S, Ruggeri A, Montes GS. Distribution of elastic system fibres in the rat tail tendon and its associated sheaths. Acta Anat. 2008;139(4):341–348. doi:10.1159/000147022.
43. VERHOEFF FH. Some new staining methods of wide applicability.: including a rapid differential stain for elastic tissue. J Am Med Assoc. 1908;L(11):876–877. doi:10.1001/jama.1908.25310370042004a.
44. Gigante A, Chillemi C, Potter KA, Bertoni-Freddari C, Greco F. Elastic fibers of musculoskeletal tissues in bovine marfan syndrome: a morphometric study. J Orthop Res. 1999;17(4):624–628. doi:10.1002/jor.1100170424.
45. Histology, verhoeff stain. Treasure Island (FL): StatPearls Publishing. Q10
46. Thorpe CT, Karunaseelan KJ, Ng Chieng Hin J, Riley GP, Birch HL, Clegg PD, Screen HRC. Distribution of proteins within different compartments of tendon varies according to tendon type. J Anat. 2016;229(3):450–458. doi:10.1111/joa.12485.
47. Abraham AC, Fang F, Golman M, Oikonomou P, Thomopoulos S. The role of loading in murine models of rotator cuff disease. J Orthop Res. 2022;40(4):977–986. doi:10.1002/jor.25113.
48. Golman M, Birman V, Thomopoulos S, Genin GM. Enthesis strength, toughness and stiffness: an image-based model comparing tendon insertions with

varying bony attachment geometries. J R Soc Interface. 2021;18(185):20210421. doi:10.1098/rsif.2021.0421.

49. Tendon enthesis mechanical failure mechanisms. Transactions of the 62st meeting of the Orthopaedic Research Society. Orlando, FL: date. Q11

50. Kurtaliaj I, Golman M, Abraham AC, Thomopoulos S. Biomechanical testing of murine tendons. J Vis Exp. 2019; 152. Q12

51. Dempster DW, Compston JE, Drezner MK, Glorieux FH, Kanis JA, Malluche H, Meunier PJ, Ott SM, Recker RR, Parfitt AM. Standardized nomenclature, symbols, and units for bone histomorphometry: a 2012 update of the report of the asbmr histomorphometry nomenclature committee. J of Bone & Mineral Res. 2013;28(1):2–17. doi:10.1002/jbmr.1805.

52. Parfitt AM, Drezner MK, Glorieux FH, Kanis JA, Malluche H, Meunier PJ, Ott SM, RR R. Bone histomorphometry: standardization of nomenclature, symbols, and units. Report of the asbmr histomorphometry nomenclature committee. J Bone Miner Res. 1987;2(6):595–610. doi:10.1002/jbmr.5650020617.

53. Moody M, Peterson A, Wingender B, Morozov K, Nakashima I, Easson M, Abraham R, Schmidt TA, Caromile L, Deymier AC. 2023. Murine bone exhibits temporal response to metabolic acidosis. Front Physiol. Submitted(. 10.2139/ssrn.4111775.

54. Frassetto L, Banerjee T, Powe N, Sebastian A. Acid balance, dietary acid load, and bone effects-a controversial subject. Nutrients. 2018;10(4):517. doi:10.3390/nu10040517.

55. Bushinsky DA, Chabala JM, Gavrilov KL, Levi-Setti R. Effects of in vivo metabolic acidosis on midcortical bone ion composition. Am J Physiol-Renal. 1999;277(5):F813–F819. doi:10.1152/ajprenal.1999.277.5.F813.

56. Meghji S, Morrison MS, Henderson B, Arnett TR. Ph dependence of bone resorption: mouse calvarial osteoclasts are activated by acidosis. Am J Physiol Endocrinol Metab. 2001;280(1):E112–E119. doi:10.1152/ajpendo.2001.280.1.E112.

57. Arnett TR, Spowage M. Modulation of the resorptive activity of rat osteoclasts by small changes in extracellular ph near the physiological range. Bone. 1996;18(3):277–279. doi:10.1016/8756-3282(95)00486-6.

58. Dekanić D. The effect of chronic acidosis on bone composition in adult male and female rats. Arh Hig Rada Toksikol. 1979;30(1):15–23.

59. Kraut JA, Coburn JW. Bone, acid, and osteoporosis. N Engl J Med. 1994;330(25):1821–1822. doi:10.1056/NEJM199406233302510.

60. Tao Z, Liu W, Ma W, Luo P, Zhi S, Zhou R. A simultaneous bilateral quadriceps and patellar tendons rupture in patients with chronic kidney disease undergoing long-term hemodialysis: a case report. BMC Musculoskelet Disord. 2020;21(1):179. doi:10.1186/s12891-020-03204-6.

61. Lotem M, Zeelenfreund M, Fried A, Robson MD, Goldschmidt Z, Rosenfeld JB. Spontaneous rupture of the quadriceps tendon in renal failure and long-term haemodialysis. Int Orthop. 1977;1(2):149–151. doi:10.1007/BF00576319.

62. Mu C, Li D, Lin W, Ding Y, Zhang G. Temperature induced denaturation of collagen in acidic solution. Biopolymers: Original Research On Biomolecules. 2007;86(4):282–287. doi:10.1002/bip.20742.

63. Li Y, Asadi A, Monroe MR, Douglas EP. Ph effects on collagen fibrillogenesis in vitro: electrostatic interactions and phosphate binding. Mater Sci Eng: C. 2009;29(5):1643–1649. doi:10.1016/j.msec.2009.01.001.

64. Russell AE. Effect of pH on thermal stability of collagen in the dispersed and aggregated states (short communication). Biochem J. 1974;139(1):277. doi:10.1042/bj1390277.

65. Flanagan CD, Unal M, Akkus O, Rimnac CM. Raman spectral markers of collagen denaturation and hydration in human cortical bone tissue are affected by radiation sterilization and high cycle fatigue damage. J Mech Behav Biomed Mater. 2017;75:75(314–321. doi:10.1016/j.jmbbm.2017.07.016.

66. Frick KK, Jiang L, Bushinsky DA. Acute metabolic acidosis inhibits the induction of osteoblastic egr-1 and type 1 collagen. Am J Physiol. 1997;272(5 Pt 1):C1450–1456. doi:10.1152/ajpcell.1997.272.5.C1450.

67. Fields M, Spencer N, Dudhia J, McMillan PF. Structural changes in cartilage and collagen studied by high temperature raman spectroscopy. Biopolymers. 2017;107(6):e23017. doi:10.1002/bip.23017.

68. Movasaghi Z, Rehman S, Rehman IU. Raman spectroscopy of biological tissues. Appl Spectrosc Rev. 2007;42(5):493–541. doi:10.1080/05704920701551530.

69. Bugarski M, Ghazi S, Polesel M, Martins JR, Hall AM. Changes in nad and lipid metabolism drive acidosis-induced acute kidney injury. J Am Soc Nephrol. 2021;32(2):342–356. doi:10.1681/ASN.2020071003.

70. Frushour BG, Koenig JL. Raman scattering of collagen, gelatin, and elastin. Biopolymers. 1975;14(2):379–391. doi:10.1002/bip.1975.360140211.

71. Finlayson GR, Smith JG Jr., Moore MJ. Effects of chronic acidosis on connective tissue. JAMA. 1964;187(9):659–662. doi:10.1001/jama.1964.03060220033010.

72. Bendeck MP, Langille BL. Rapid accumulation of elastin and collagen in the aortas of sheep in the immediate perinatal period. Circ Res. 1991;69(4):1165–1169. doi:10.1161/01.RES.69.4.1165.

73. Richardson BS, Carmichael L, Homan J, Tanswell K, Webster AC. Regional blood flow change in the lamb during the perinatal period. Am J Obstet Gynecol. 1989;160(4):919–925. doi:10.1016/0002-9378(89)90311-6.

74. Deymier AC, Nair AK, Depalle B, Qin Z, Arcot K, Drouet C, Yoder CH, Buehler MJ, Thomopoulos S, Genin GM, Pasteris JD, et al. Protein-free formation of bone-like apatite: new insights into the key role of carbonation. Biomaterials. 2017;127:127(75–88.

75. Unal M, Uppuganti S, Timur S, Mahadevan-Jansen A, Akkus O, Nyman JS. Assessing matrix quality by raman spectroscopy helps predict fracture toughness of human cortical bone. Sci Rep. 2019;9(1):7195–7195. doi:10.1038/s41598-019-43542-7.

76. Bailey AJ. Molecular mechanisms of ageing in connective tissues. Mech Ageing Dev. 2001;122(7):735–755. doi:10.1016/S0047-6374(01)00225-1.

77. Currey JD. Bones: structure and mechanics. Princeton, NJ: Princeton University Press. Q13